Nature Communications

https://doi.org/10.1038/s41467-026-71872-4

Article in Press

A molecular framework of the *Rht-A1–TaLA1-D* module controlling tiller angle in wheat

Received: 3 September 2025

Accepted: 1 April 2026

Cite this article as: Chen, Y., Xie, Z., Dong, C. *et al.* A molecular framework of the *Rht-A1–TaLA1-D* module controlling tiller angle in wheat. *Nat Commun* (2026). https://doi.org/10.1038/s41467-026-71872-4

Yaoyu Chen, Zhencheng Xie, Chunhao Dong, Danping Li, Hao Cheng, Baolian Lv, Chuan Xia, Jiaqiang Sun, Xu Liu, Xiuying Kong & Lichao Zhang

A molecular framework of the *Rht-A1–TaLA1-D* module controlling tiller angle in wheat

Yaoyu Chen[1], Zhencheng Xie[1], Chunhao Dong[1,2], Danping Li[1,3], Hao Cheng[1], Baolian Lv[1], Chuan Xia[1], Jiaqiang Sun[1,*], Xu Liu[1,*], Xiuying Kong[1,*] & Lichao Zhang[1,*]

[1]State Key Laboratory of Crop Gene Resources and Breeding, Institute of Crop Sciences, Chinese Academy of Agricultural Sciences, Beijing 100081, China.

[2]College of Agronomy, Henan Agricultural University, Zhengzhou 450046, China.

[3]Crop Research Institute, Shandong Academy of Agricultural Sciences, Jinan 250100, China.

*Authors for correspondence: Jiaqiang Sun, Xu Liu, Xiuying Kong and Lichao Zhang

e-mail: sunjiaqiang@caas.cn; liuxu03@caas.cn; kongxiuying@caas.cn; zhanglichao@caas.cn

Abstract

Tiller angle is a critical determinant of wheat plant architecture, which profoundly impacts yield potential. However, the regulatory mechanisms of tiller angle in wheat remain largely unexplored. To explore the underlying mechanisms, we identify two EMS-mutagenized wheat mutants *tiller angle 1* (*ta1*) and *ta2* with enlarged tiller angles. Molecular characterization reveals that *TA1* and *TA2* encode the DELLA protein Rht-A1 and TaLA1-D, respectively. Biochemical analyses demonstrate that the Rht-A1^{ta1} variant acquires enhanced protein stability, whereas TaLA1-D^{ta2} exhibits destabilization. We establish a mechanistic framework that Rht-A1 physically associates with TaPROG1 to synergistically repress *TaLA1-D* transcription. Moreover, we show that TaGSK3 directly

interacts with and phosphorylates TaLA1-D to enhance its stability in reducing wheat tiller angles. Population genomic analyses uncover a significant selection for the elite *TaLA1-D*^{Hap1} allele during modern wheat breeding, correlating with compact plant architecture and elevated thousand-grain weight. This study provides new insights into plant architecture regulation and target genes for improving yield potential in wheat.

Introduction

Wheat (*Triticum aestivum* L.) is the most widely cultivated cereal crop globally, which supplies approximately 20% of human caloric intake and serves as a primary protein source worldwide[1,2]. With the global population increasing, meeting the escalating demand for wheat production represents a critical agricultural challenge[3,4]. The Green Revolution of the 1960s addressed this challenge through the introduction of semi-dwarfing genes *Rht-B1b* and *Rht-D1b* encoding stabilized DELLA proteins, which improved lodging resistance and harvest index by optimizing plant height[5]. However, beyond plant height, tiller angle constitutes another crucial architectural determinant influencing light interception efficiency and yield potential[6,7].

Recent advances in rice (*Oryza sativa* L.) have identified key genetic regulators of tiller angle[8], including *LAZY1* (*LA1*)[9] and *TILLER ANGLE CONTROL 1* (*TAC1*)[10], both encoding members of the IGT protein family[11,12]. While *LA1* loss-of-function mutants display dramatically increased tiller angles[13], *TAC1* overexpression causes lateral shoot spreading[14,15]. The C2H2 zinc finger transcription factor PROSTRATE GROWTH 1 (PROG1) also regulates tiller angle, with its functional loss contributing to the erect growth habit characteristic of domesticated rice[16,17]. Notably, these regulators controlling tiller angle in rice are predominantly associated with the auxin pathway[8,18,19]. However, studies on the roles of other phytohormones, such as gibberellin (GA) and brassinosteroids (BR), in modulating tiller angle remain relatively limited. Despite these insights into rice, the

genetic control of tiller angle in wheat remains poorly understood[20,21]. To date, only a few genes, such as *TaTAC-D1*[22] and *TaHST1L/TaTAC-A1*[23], have been reported to regulate tiller angle in wheat. We previously identified *Reduced height-B1* (*Rht-B1*), which encodes a DELLA protein in the GA signaling pathway, as a regulator of this trait[24]. Despite these findings, the underlying molecular mechanisms control tiller angle in wheat remains unclear.

Here, we characterize two wheat tiller angle mutants (*ta1* and *ta2*) to unravel a regulatory module integrating phytohormone signaling and tiller angle. We demonstrate that: *TA1* encodes the DELLA protein Rht-A1, which physically interacts with TaPROG1 to transcriptionally repress *TA2*/*TaLA1-D* expression. Moreover, TaGSK3-mediated phosphorylation enhances the stability of TaLA1-D. Population genetics reveals a significant selection for *TaLA1-D*^{Hap1} alleles with smaller tiller angles during wheat breeding.

Results

Identification of *ta1* and *ta2* mutants showing enlarged tiller angles

To explore the regulatory mechanism of tiller angle in wheat, we screened ethyl methane sulfonate (EMS)-induced mutant libraries in the Yanzhan4110 (YZ4110) and Huaimai (HM33) backgrounds. Two mutants, *ta1* and *ta2*, were identified with significantly increased tiller angles (Fig. 1a and 1b). Across all developmental stages, the *ta1* mutant consistently displayed a larger tiller angle than YZ4110 under greenhouse conditions and field trials (Supplementary Figs. 1, 2), peaking at ~49° during the elongation stage and gradually declining thereafter, ultimately reaching ~33° at the grain filling stage compared to ~20° in YZ4110 under field conditions (Fig. 1c). Additionally, the *ta1* mutant exhibited a notable reduction in plant height (Fig. 1d) and a severely diminished shoot gravitropic response at the seedling stage (Fig. 1e, f). Similarly, the *ta2* mutant showed an increased

tiller angle compared to HM33 (Fig. 1g), accompanied by a moderate reduction in plant height and an impaired shoot gravitropic response (Fig. 1h–j).

Map-based cloning of *TA1* that encodes the DELLA protein Rht-A1

To understand the genetic basis of the enlarged tiller angle phenotype in the *ta1* mutant, we conducted genetic analyses using the populations by genetic crosses between *ta1* and YZ4110 or HM33. The $BC_2F_{2:3}$ population (237 lines) derived from the genetic cross between *ta1* and YZ4110 showed a bimodal segregation fitting a 3:1 ratio (normal tiller angle: enlarged tiller angle) in the tiller angle (Supplementary Fig. 3), suggesting that the enlarged tiller angle phenotype of *ta1* mutant is likely caused by a single dominant mutation.

To identify the causal gene for the enlarged tiller angle of the *ta1* mutant, we performed fine-mapping combined with 55 K SNP microarray genotyping and whole-exome sequencing (WES). The 55 K SNP microarray analysis revealed chromosome 4A as the most polymorphic region (Fig. 2a). Using six derived KASP markers, we mapped the candidate locus to a 54-Mb interval (542 Mb - 596 Mb) on chromosome 4A through linkage analysis of a 453-individual F_2 population (*ta1* × HM33) (Fig. 2b). Subsequent fine-mapping with five additional markers in an expanded F_2 population (n = 1344) narrowed the *TA1* locus to a 1-Mb region (581 Mb - 582 Mb) (Fig. 2c; Supplementary Data 1), an interval containing 22 high-confidence genes (Supplementary Data 2). Although WES and whole-genome resequencing identified sequence variations in five genes, only a G-to-A mutation in *TraesCS4A02G271000 (Rht-A1*) resulted in an amino acid change in the functionally essential DELLA domain (Fig. 2d). Genotyping in the F_2 population showed that this mutation co-segregated with tiller angle, with the “A” allele conferring a significantly larger angle than the “G” allele (Supplementary Fig. 4). Functional characterization indicated that this mutation ($Rht\text{-}A1^{ta1}$) led to a reduction in GA-mediated DELLA protein degradation (Fig. 2e; Supplementary Fig. 5) and the DELLA

protein was substantially accumulated in the *ta1* mutant compared to YZ4110 (Supplementary Fig. 6), thereby supporting it as the causal mutation underlying the *ta1* phenotype.

To validate the role of *Rht-A1*^{ta1} in regulating tiller angle, we generated transgenic wheat lines expressing *Rht-A1*^{ta1} under its native promoter (*pRht-A1::Rht-A1*^{ta1}) and the constitutive maize *Ubiquitin* promoter *(pUbi::Rht-A1*^{ta1}), respectively. Transgenic plants containing both constructs exhibited significantly increased tiller angles and reduced plant height compared to wild-type controls (Fig. 2f, g; Supplementary Fig. 7a, b). Notably, *pUbi::Rht-A1*^{ta1} lines showed more significant phenotypic alterations than *pRht-A1::Rht-A1*^{ta1} lines, consistent with the stronger expression driven by the *Ubiquitin* promoter (Supplementary Fig. 7c). These results conclusively confirmed *Rht-A1* as the *TA1* gene responsible for tiller angle regulation in wheat.

Given that the YZ4110 wheat cultivar carries the gain-of-function *Rht-D1b* allele (Supplementary Data 3), the *ta1* mutant in this genetic background represents a double mutant combining *Rht-A1*^{ta1} and *Rht-D1b*. To systematically evaluate the individual and combined effects of *Rht-A1*^{ta1}, *Rht-B1b*, and *Rht-D1b* alleles on wheat architecture, we generated a BC_1F_5 population by crossing the *ta1* mutant (*Rht-A1*^{ta1}*/Rht-D1b*) with a wheat plant harboring *Rht-B1b*. From this population, we identified a panel of wheat progenies to detect the genetic effects of *Rht-1* alleles (Fig. 2h). Field evaluation revealed distinct phenotypic patterns: single *Rht-1* alleles *(Rht-A1*^{ta1}, *Rht-B1b*, or *Rht-D1b*) moderately reduced plant height without affecting tiller angle, whereas the different double mutants of these alleles could increase tiller angle (Fig. 2i). Most notably, the triple mutant exhibited synergistic effects, displaying severely enlarged tiller angles and dramatically reduced plant height (Fig. 2i, j). Moreover, we found that exogenous application of the gibberellin biosynthesis inhibitor paclobutrazol (PAC) increased tiller angle in wheat (Supplementary Fig. 8a, b). Consistently, gene editing of three *TaGA3ox2* homoeologous genes (*TraesCS3A02G122600*, *TraesCS3B02G141800* and

TraesCS3D02G124500) led to an enlarged tiller angle phenotype and this phenotype could be rescued by external application of GA_3 (Supplementary Fig. 8c, d). These results demonstrate that gibberellin negatively regulates tiller angle in wheat.

Map-based cloning of *TA2* that encodes TaLA1-D

To clone the *TA2* gene, we performed bulked segregant analysis (BSA)-sequencing using pooled DNA from plants with normal and enlarged tiller angles, respectively, of the F_2 populations generated by the genetic crosses between *ta2* and HM33 or JM22. These bulked DNA samples were used for 55 K microarray genotyping (JM22 background) and whole-exome sequencing (HM33 background). The results showed that the largest number of SNPs were enriched on chromosome 6DL (Fig. 3a, Supplementary Fig. 9). Using these SNPs, 9 markers were developed to screen 94 homozygous *ta2* mutants, validated through the $F_{2:3}$ population of the genetic cross between *ta2* and JM22 (Supplementary Data 4). The candidate locus was delimited to a ~2 Mb interval on chromosome 6DL (467-469 Mb), containing 40 high-confidence genes (Supplementary Data 5). WES and whole-genome resequencing of extreme-phenotype individuals identified four genes with sequence variations. Notably, *TaLA1-D* (*TraesCS6D02G396500*), the wheat ortholog of rice *LA1*, carried a missense variant: a G-to-A mutation in its third exon causing a glycine-to-aspartic acid substitution (Fig. 3b). In the F_2 population, this mutation co-segregated with phenotype: plants homozygous for the mutant “A” allele exhibited a significantly larger tiller angle than those with the wild-type “G” allele (Supplementary Fig. 10). In order to investigate how the substitution of glycine-to-aspartic acid on the TaLA1-D affects its function, we conducted subcellular localization and protein stability analyses for this protein. The results showed that although the TaLA1-D^{ta2} variant maintained normal subcellular localization (Supplementary Fig. 11), its protein stability was reduced (Fig. 3c).

To confirm the role of *TaLA1* in tiller angle regulation, we generated knockout mutants of *TaLA1* in the KN199 background using CRISPR/Cas9 (Supplementary Fig. 12a). As expected, these mutants displayed significantly increased tiller angles alongside a decrease in thousand-kernel weight compared to wild-type plants (Fig. 3d, e; Supplementary Fig. 12b; Supplementary Fig. 13). Additionally, we identified a premature stop codon mutant of *TaLA1-D* (*Tala1-D*^{C34T}) from an EMS mutant library in the wheat cultivar JM38 background, which also exhibited a larger tiller angle phenotype (Supplementary Fig. 14). These results confirmed that *TaLA1-D* is involved in the regulation of tiller angles in wheat.

To explore the mechanism of *TaLA1* in regulating wheat tiller angles, we measured the auxin levels in the tiller base. The results showed that the auxin level was reduced in the *CRISPR-Tala1* mutants compared with KN199 (Fig. 3f). Transcriptome and RT–qPCR analyses revealed significantly reduced expression levels of multiple *expansin* (*EXP*) genes and *xyloglucan endotransglucosylase/hydrolase* (*XTH*) genes in the *CRISPR-Tala1* mutants (Supplementary Fig. 15; Fig. 3g, h). These results suggest that *TaLA1-D* regulates tiller angle potentially through affecting auxin level and the expression of cell wall-loosening related genes in wheat.

Rht-A1 interacts with the transcription factor TaPROG1 to synergistically repress *TaLA1-D* expression

Molecular characterization revealed that the DELLA protein Rht-A1 (TA1) negatively regulates *TaLA1-D* (*TA2*) expression, as evidenced by significantly reduced *TaLA1-D* transcript levels in the gain-of-function mutant *ta1* and the *Rht-A1*^{ta1} overexpression transgenic plants (Fig. 4a; Supplementary Fig. 16). Then, the dual-luciferase reporter analysis, yeast one-hybrid (Y1H) and ChIP-qPCR assays demonstrated that TaPROG1 (TraesCS5A02G511400) could directly bind to the promoter of *TaLA1-D* to repress its expression (Fig. 4b, c; Supplementary Fig. 17). Furthermore, the transient expression

assays showed that Rht-A1 and TaPROG1 synergically repress the transcriptional expression of *TaLA1-D* (Supplementary Fig. 18). Consistently, overexpression of *TaPROG1* increased tiller angle and reduced *TaLA1* expression (Supplementary Figs. 19, 20). Based on the above results, we wondered whether Rht-A1 interacts with TaPROG1 to repress the expression of *TaLA1-D* in wheat. The luciferase complementation imaging (LCI) and bimolecular fluorescence complementation (BiFC) assays demonstrated that Rht-A1 could physically interact with TaPROG1 (Fig. 4d, e). Further analysis revealed that this interaction enhances the stability of the TaPROG1 protein in *Rht-A1^{ta1}* overexpression plants (Supplementary Fig. 21).

To genetically characterize the functional relationship between Rht-A1 and TaPROG1 in the regulation of *TaLA1-D* expression, we generated the *TaPROG1* and *Rht-A1^{ta1}* double-transgenic plants. Phenotypic characterization showed that these transgenic plants displayed significantly larger tiller angles and markedly reduced plant height compared with the single-transgenic plants (Fig. 4f). Furthermore, we found that the expression levels of *TaLA1-D* were remarkably reduced in the double-transgenic plants compared with those in the single transgenic plants (Fig. 4g). These results demonstrated that the DELLA protein Rht-A1 and TaPROG1 synergistically repress the expression of *TaLA1-D* to regulate tiller angle in wheat.

In addition, we showed that overexpression of *TaPROG1* also reduced plant height in wheat (Supplementary Fig. 19). Considering that GA is a key phytohormone in the regulation of plant height, we checked the expression levels of gibberellin biosynthetic genes in the *pUbi::TaPROG1* transgenic plants. Y1H and dual-luciferase reporter assays demonstrated that TaPROG1 could directly bind to the promoter of *TaGA3ox2* (*TraesCS3D02G124500*) to repress its expression (Supplementary Fig. 22a–c). As expected, the active GAs (GA_1 and GA_4) levels were remarkably reduced and thus the DELLA proteins were over-accumulated in the *pUbi::TaPROG1* transgenic plants (Supplementary Fig. 22d, e). Additionally, exogenous application of GA_3 could partially

rescue the enlarged tiller angle phenotype of the *pUbi::TaPROG1* transgenic plants (Supplementary Fig. 22f, g). These findings establish a positive feedback loop wherein TaPROG1 enhances the protein stability of Rht-A1 through directly repressing the gibberellin biosynthesis, which in turn cooperates with TaPROG1 to repress *TaLA1-D* expression.

TaGSK3 phosphorylates and enhances the stability of TaLA1-D to regulate wheat tiller angle

Our previous study showed that the *Tagsk3*^{E286K} mutant of *TaGSK3*, a crucial negative regulator of brassinosteroid signaling, exhibits compact plant architecture[25]. Here, we observed that the *TaGSK3*^{E286K}-overexpressing plants displayed significantly reduced tiller angles compared with the wild-type KN199 (Fig. 5a, b), prompting us to test whether TaGSK3 interacts with TaLA1-D. To this end, we performed the protein-protein interaction assays using the yeast two-hybrid (Y2H), BiFC and LCI. The results demonstrated that TaGSK3 could directly interact with TaLA1-D (Fig. 5c–e). Since TaGSK3 is a serine/threonine kinase[25-27], we wanted to know whether TaGSK3 could phosphorylate TaLA1-D protein. As shown in Fig. 5f, both the TaLA1-D^{N}-MBP and TaLA1-D^{C}-MBP incubation with TaGSK3-GST generated slowly migrating bands in the Phos-tag gel, indicating that TaLA1-D could be phosphorylated by the TaGSK3 kinase. Further, cell-free degradation assays revealed delayed TaLA1-D degradation in TaGSK3-overexpressing lines (Fig. 5g), indicating that TaGSK3-mediated phosphorylation enhances TaLA1-D protein stability. Furthermore, genetic analysis showed that the *TaGSK3*^{E286K}-overexpression transgenic plants in the *CRISPR-Tala1* genetic background displayed an enlarged tiller angle phenotype, similar to the single mutant *CRISPR-Tala1* (Fig. 5h, i). Consequently, within the genetic pathway regulating tiller angle, TaGSK3 likely functions upstream of *TaLA1*. Taken together, the above results reveal a regulatory

mechanism for the TaLA1-D stability by TaGSK3-mediated phosphorylation in the control of wheat tiller angle.

The elite *TaLA1-D*^{Hap1} allele was selected for yield traits during wheat breeding

To evaluate the breeding values of *TaLA1-D*, we first performed sequence analyses of *TaLA1-D* using the 83 diverse wheat accessions (50 landraces and 33 modern cultivars) collected by our research group. According to 5 SNP in the promoter region of *TaLA1-D*, the Hap1, Hap2 and Hap3 haplotypes were identified (Fig. 6a). Strikingly, we found that modern wheat cultivars harbor only Hap1, while all the three haplotypes were distributed in the landraces (Fig. 6b), suggesting a strong artificial selection for Hap1 during modern wheat improvement. Moreover, accessions carrying Hap1 not only displayed reduced tiller angels and larger grain size but also achieved a corresponding increase in thousand-grain weight of at least 28.4% (Fig. 6c–f). Additionally, we extended the haplotype analysis to 1,351 wheat accessions from the wheat re-sequencing project[3,28-31]. We found that the *TaLA1-D*^{Hap1} haplotype was harbored in 91.1% of the modern wheat cultivars but only in 74.0% of the landraces among the 1,351 accessions (Supplementary Fig. 23). Chi-square analysis supported that the elite *TaLA1-D*^{Hap1} haplotype had been significantly selected during modern wheat breeding ($\chi^2 = 50.79$, df = 1, $P < 0.0001$). Further population genetic analysis indicated strong positive selection on *TaLA1-D* during modern wheat breeding, as shown by significantly reduced nucleotide diversity (π) and elevated population differentiation (F_{ST}) in cultivars versus landraces (Supplementary Fig. 24). Beyond the target gene itself, we detected clear selection signatures for advantageous haplotypes of two key upstream regulators: *TaPROG1*^{Hap1} and *TaGSK3*^{Hap1} (Supplementary Figs. 25, 26).

Discussion

Tiller angle is a crucial agronomic trait that influences wheat yield potential by modulating canopy photosynthetic efficiency[8]. Despite its importance, the genetic basis of tiller angle regulation in wheat remains poorly understood[18,19]. Our study addresses this gap by identifying two tiller angle regulators in wheat: the DELLA protein Rht-A1^{ta1} and the IGT protein TaLA1-D that is functionally opposite to another IGT protein TaTAC1. (Figs. 1–3). We further elucidate a comprehensive molecular framework in which the *Rht-A1–TaLA1-D* module is responsible for tiller angle regulation in wheat (Fig. 7).

In line with its orthologue in rice[19,32], TaPROG1 directly represses the expression of *TaLA1-D* in wheat (Fig. 4b, c; Supplementary Figs. 17, 20). Furthermore, Rht-A1 suppresses *TaLA1-D* by interacting with and potentiating the repressor activity of TaPROG1 (Fig. 4). This repression regulation may be reinforced by a positive feedback loop wherein TaPROG1 directly represses gibberellin biosynthesis thereby causing the accumulation of DELLA proteins (Supplementary Fig. 22). This feedback loop ensures efficient repression of *TaLA1-D* transcription to fine-tune tiller angle in wheat. On the other hand, we revealed that TaGSK3-mediated phosphorylation could enhance the protein stability of TaLA1-D (Fig. 5). Alterations in the different components of this regulatory network shape distinct tiller angle phenotypes in wheat: in the *ta1* mutant, the accumulated Rht-A1^{ta1} proteins enhance the TaPROG1-mediated repression of *TaLA1-D* expression, thereby promoting enlarged tiller angles; in the *Tala1-D* mutant, disruption of *TaLA1-D* results in increased tiller angles; in the *Tagsk3*^{E286K} mutant/transgenic plants, the accumulated TaGSK3 proteins enhance the protein stability of TaLA1-D, yielding a compact plant architecture with smaller tiller angles (Fig. 7).

Notably, while *Rht-B1b* and *Rht-D1b* alleles drove the Green Revolution, their *Rht-A1* counterpart remained unexplored. We characterized a functionally important semi-dwarfing allele of *Rht-A1* (*Rht-A1*^{ta1}), which confers more severe height reduction than *Rht-B1b* or *Rht-D1b* (Fig. 2h–j). Intriguingly, while single alleles moderately reduced plant height without affecting tiller angles, their combinations enlarged tiller angles. This result

suggests that in wheat, fine-tuning of GA signaling can coordinately regulate both plant height and tiller angle. This coordinated regulation appears distinct from that in rice, where GA is well-known to control plant height[33-35], but its role in tiller angle regulation remains unclear.

Comparative phytohormone analysis revealed opposing effects of BR and GA on tiller angle. BR positively regulates tiller angle: BR deficiency (via the *D2* mutation[36]) or signaling enhancement (via *OsLIC* suppression[37] or the gain-of-function of *TaGSK3*[25]) decreases or increases tiller angles, respectively. In contrast, GA negatively regulates tiller angle: the suppression of GA signaling through stabilized DELLA proteins enlarges tiller angle, as demonstrated here and in our previous study[24]. The *TaPROG1*-mediated reduction in active GA levels further stabilizes DELLA proteins, forming a self-reinforcing loop. Whether this loop is modulated by other hormones (e.g., BR) needs further investigation. We further established that TaLA1 regulates tiller angle via the auxin pathway in wheat (Fig. 3f), consistent with the conserved function of LA1 in rice[13]. Thus, the *Rht-A1–TaLA1-D* module integrates multiple hormonal pathways, including gibberellin, brassinosteroid and auxin, to coordinately control tiller angle in wheat.

Overall, the identification of *Rht-A1–TaLA1-D* module represents a critical advance in deciphering the regulatory network of tiller angle in wheat. By taking advantage of natural and engineered variations in these components, it is possible to design elite wheat varieties with optimal tiller angles for high-yield potential in future wheat breeding.

Methods

Plant materials and growth conditions

Two tiller angle mutants (*ta1* and *ta2*) were isolated from ethyl methanesulfonate (EMS)-mutagenized populations of wheat (*Triticum aestivum* L.) cultivars YZ4110 and HM33, respectively. The *ta1* mutant was crossed with YZ4110, and YZ4110 was used as the recurrent parent to generate the YZ4110×*ta1* $BC_2F_{2:3}$ progenies. The *ta1* mutant was

crossed with Fielder, and Fielder was used as the recurrent parent to generate the Fielder×*ta1* BC_1F_5 progeny. The *ta2* mutant was crossed with HM33 and JM22 to generate their F_2 progenies. Field evaluations were conducted at Xinxiang, China (34°N, 113°E).

The 83 diverse wheat accessions, including 50 landraces and 33 modern cultivars, were cultivated and characterized for two years (2020–2022) at Xinxiang, China. These wheat accessions are listed in Supplementary Data 6.

The wheat cultivar KN199 was used for genetic transformation. Transgenic plants were grown under controlled greenhouse conditions (25/20°C day/night, 16 h photoperiod, 50 μmol $m^{-2}·s^{-1}$) or in field trials at Beijing, China (39°N, 116°E). For transient assays, *Nicotiana benthamiana* plants were maintained in growth chambers (23°C, 65% RH, 17 h photoperiod).

Tiller angle measurement

Tiller angles were measured throughout wheat development using stage-specific protocols. During vegetative stages (seedling to elongation), angles were measured directly using a 180° protractor. For reproductive stages (post-elongation to maturity), we quantified the maximum tiller inclination by measuring the horizontal displacement between the vertical line and the most angled tiller at 30 cm above ground level, then calculating the angle using arctangent function.

Gravitropic response analysis

Wheat seeds were surface sterilized with 10% (v/v) sodium hypochlorite for 15 min, rinsed thoroughly with distilled water, then germinated on moist filter paper in petri dishes at 25°C. After 24 h, seedlings with equivalent radicle emergence (2–3 mm) were selected and transplanted into 50 mL conical tubes containing 0.45% (w/v) agar medium. Following 48 h of vertical growth in the dark, tubes were rotated 90° to initiate gravistimulation.

Gravitropic curvature was quantified by measuring the angle between the shoot apex and vertical axis using a 180° protractor when seedlings were reoriented 90° for 48 h.

Gibberellin treatment assays

Fifteen-day-old seedlings were selected for gibberellin or gibberellin biosynthesis inhibitor paclobutrazol (PAC) treatments. The wheat cultivar KN199 seedlings were continuously sprayed with 100 μM GA_3 (Sigma, Cat. No. G1025) or 100 μM PAC (Sangon, Cat. No. A630332) every 24 h for one month. The *TaPROG1*-overexpression transgenic plants and the *TaGA3ox2* gene-edited mutants were continuously sprayed with 100 μM GA_3 every 24 h for one month.

RNA extraction and RT–qPCR

For RNA extraction and reverse transcription, we performed the following procedures: Total RNA was extracted from various tissue samples using TRIzol™ Reagent (Invitrogen, Cat. No. 15596018) following the manufacturer's protocol. RNA quality and concentration were verified by spectrophotometry. First-strand cDNA synthesis was carried out using 1 μg of total RNA with the 5× All-In-One RT MasterMix system (Applied Biological Materials Inc., Cat. No. G592) under optimized thermal cycling conditions: 37°C for 15 minutes for reverse transcription, 60°C for 10 minutes for enzyme inactivation, and 95°C for 3 minutes for final denaturation. The resulting cDNA products were diluted 1:5 with nuclease-free water before subsequent analysis.

Quantitative real-time PCR was performed using SYBR Premix Ex Taq™ (TaKaRa, Cat. No. RR420A) on a LightCycler96 (Roche). Each 10 μL reaction contained 1 μL of diluted cDNA template. The thermal cycling protocol consisted of an initial denaturation at 95°C for 1 minute, followed by 40 cycles of amplification (95°C for 5 seconds and 60°C for 30 seconds). Melting curve analysis was conducted to verify amplification specificity. Three biologically independent replicates were performed, and relative gene expression

levels were calculated using the $2^{-\Delta\Delta Ct}$ methods with *TaActin* was used as control. The primers used for RT–qPCR are listed in Supplementary Data 7.

Transgenic plant generation

For *Rht-A1^{ta1}* gene constructs, we amplified a 5,469-bp genomic DNA fragment (including 2249-bp promoter region, 1863-bp gene body and 1357-bp downstream sequence from the terminator codon) of *Rht-A1^{ta1}* from the *ta1* mutant. This fragment, along with a 1,860-bp coding sequence, was independently cloned into the pWMB110 vector[31] and transformed into the wheat cultivar KN199 using Agrobacterium-mediated transformation, generated *pRht-A1::Rht-A1^{ta1}* and *pUbi::Rht-A1^{ta1}*-Flag transgenic lines respectively.

For *TaPROG1* (*TraesCS5A02G511400*) overexpression, we identified the coding sequence through homology searches using rice *PROG1* (*Os07g0153600*) as query in the Ensembl Plants database. The 564-bp *TaPROG1* coding sequence was PCR-amplified from KN199 genomic DNA and subsequently cloned into the pWMB110 vector[24] under the control of the maize *ubiquitin* promoter, generating *pUbi::PROG1-GFP* constructs that were transformed into KN199.

For targeted genome editing of *TaLA1*, we designed two CRISPR/Cas9 guide RNAs using the WheatCrispr online tool[38] to simultaneously target homologous sequences in the A, B, and D subgenomes. These target sites were cloned into the pBUE413 vector[39] and introduced into KN199, generating the *CRISPR-Tala1* knockout mutants. The primers used for plasmid construction are listed in Supplementary Data 7.

Subcellular localization assay

The coding sequences of *TaLA1-D* and *TaLA1-D^{ta2}* were cloned into the pAN580-GFP vector[39]. Then the two constructs were transformed into wheat mesophyll protoplasts through the polyethylene glycol (PEG)-mediated method[40], with the empty pAN580-GFP vector serving as the negative control. After incubation in darkness at 25°C for 16 h, the

GFP fluorescence was analyzed by a confocal laser scanning microscope (Carl Zeiss, LSM900) with excitation/emission settings of 488 nm/507 nm. The primers used for plasmid construction are listed in Supplementary Data 7.

Luciferase complementation imaging (LCI)

The coding sequences of *Rht-A1* and *TaGSK3* (*TraesCS3D02G137200*) were inserted into pCAMBIA1300-nLUC, while *TaPROG1* and *TaLA1-D* were cloned into pCAMBIA1300-cLUC[39]. All constructs were introduced into Agrobacterium tumefaciens GV3101. Bacterial suspensions (OD600 = 0.8) containing different plasmid combinations were co-infiltrated into abaxial leaf surfaces of 28-day-old *N. benthamiana* plants. Luciferase activity was quantified 48 hours post-infiltration using the NightSHADE LB 985 system (Berthold Technologies). The primers used for plasmid construction are listed in Supplementary Data 7.

Bimolecular fluorescence complementation (BiFC)

The coding sequences of *Rht-A1* and *TaLA1-D* were cloned into pEarlyGate201-YC vector, while *TaPROG1* and *TaGSK3* coding sequences were inserted into pEarlyGate202-YN vector using Gateway cloning. All constructs were verified by sequencing before transformation into Agrobacterium tumefaciens strain GV3101 (OD600 = 0.8). Bacterial suspensions containing different plasmid combinations (1:1 ratio) were co-infiltrated into abaxial leaf surfaces of 28-day-old *N. benthamiana* plants using needleless syringes. Infiltrated plants were maintained at 23°C under 17 h light / 7 h dark cycles for 48 h prior to imaging. Reconstituted YFP fluorescence was detected using a confocal laser scanning microscope (Carl Zeiss LSM900) with excitation/emission settings of 514 nm/527 nm. Three biological replicates were performed for each combination. The primers used for plasmid construction are listed in Supplementary Data 7.

Dual-luciferase reporter analysis

The 1,724-bp promoter sequence of *TaLA1-D* was cloned into the pGreenII 0800-LUC vector to generate the firefly luciferase (LUC) reporter construct, while the Renilla luciferase (REN) gene driven by the cauliflower mosaic virus (CaMV) 35S promoter within the same vector served as an internal control. The coding sequence of *TaPROG1* was inserted into the pAN580-GFP effector vector[39]. Reporter and effector constructs (1:5 molar ratio) were co-transfected into wheat mesophyll protoplasts using PEG-mediated transfection[40], with empty pAN580-GFP vector included as a negative control. Following 16 h incubation at 25°C in darkness, LUC and REN activities were quantified using a dual-luciferase reporter assay system (Yeasen, Cat. No. 11402ES60). Three biologically independent replicates were performed, and relative promoter activity was calculated as the LUC/REN signal ratio. The primers used for plasmid construction are listed in Supplementary Data 7.

Yeast one-hybrid assays

The coding sequence of *TaPROG1* was cloned into pB42AD vector, while the promoter sequences of *TaLA1-D* and *TaGA3ox2* were individually cloned into pLacZ vector. Constructs were verified by sequencing before co-transformation into yeast strain EGY48 (Zomanbio, Cat. No. ZC1605) using the lithium acetate method. Yeast transformants were selected on SD/-Trp-Ura agar plates for 72 h at 30°C and transferred to SD/+Gal+Raf-Trp-Ura agar plates containing X-Gal (5-bromo-4-chloro-3-indolyl-p-D-galactopyranoside) for blue color development. The primers used for plasmid construction are listed in Supplementary Data 7.

ChIP–qPCR assay

Chromatin immunoprecipitation was performed as follows. Fresh leaves (2 g) from KN199

(negative control) and *TaPROG1*-overexpression (with a GFP tag) transgenic plants were cross-linked in 1% formaldehyde for 20 min, quenched with 0.125 M glycine, and ground to a powder in liquid nitrogen. Nuclei were isolated, and chromatin was sheared by sonication to an average size of 200–500 bp. Immunoprecipitation was carried out overnight at 4°C using an anti-GFP mAb-magnetic agarose (MBL, Cat. No. D153-10). After extensive washing, the immunoprecipitated chromatin was eluted with elution buffer (0.1 M $NaHCO_3$, 1% SDS). Cross-links were reversed, and DNA was purified. Enrichment of specific promoter regions at putative TaPROG1 binding sites was quantified by qPCR. Primers used are listed in Supplementary Data 7.

Yeast two-hybrid screening

The coding sequences of *Rht-A1*, *Rht-A1^{ta1}* and *TaLA1-D* were individually cloned into pGADT7 (AD vector), while the coding sequences of *TaGID1* and *TaGSK3* were individually cloned into pGBKT7 (BD vector). Constructs were verified by sequencing before co-transformation into yeast strain Y2HGold (Zomanbio, Cat. No. ZC1602) using the lithium acetate method. Transformants were selected on synthetic defined (SD) medium lacking tryptophan and leucine (SD/-Trp/-Leu) for 72 h at 30°C. For interaction testing, eight independent colonies were resuspended in sterile water and spotted in serial dilutions (10-fold) onto SD medium lacking tryptophan, leucine, histidine, and adenine (SD/-Trp/-Leu/-His/-Ade), followed by incubation at 30°C for 72 h. Protein-protein interactions were confirmed by colony growth on this selective medium. The primers used for plasmid construction are listed in Supplementary Data 7.

Protein expression and purification

The coding sequences of *Rht-A1* from YZ4110 and its *ta1* mutant were cloned into pMAL-c5X, while *TaPROG1* from KN199 was cloned into pET-28a. The coding sequences of *TaLA1-D* variants from HM33 and *ta2* mutant were inserted into pET-28a, while two

truncated *TaLA1-D* constructs (TaLA1^{N}: 1bp - 765 bp; TaLA1^{C}: 301 bp - 1167 bp) were generated by PCR and cloned into pMAL-c5X. *TaGSK3* from YZ4110 was subcloned into pGEX-4T-1. All constructs were transformed into *Escherichia coli* strain BL21 and expressed at 16°C with shaking (90 rpm) for 14 h. Recombinant proteins were purified using affinity chromatography according to their fusion tags. His-tagged proteins (TaLA1, TaLA1^{ta2} and TaPROG1) were isolated using IDA-Ni resin (Beaver, 70501). MBP-fused proteins (Rht-A1, Rht-A1^{ta1}, TaLA1^{C}, and TaLA1^{N}) were purified with amylose resin (NEB, E8021V). GST-tagged TaGSK3 was captured using glutathione magnetic beads (Beaver, 70601). The primers used for plasmid construction are listed in Supplementary Data 7.

In vitro protein degradation

Total proteins were extracted from 14-day-old KN199, *pRht-A1::Rht-A1^{ta1}* or *pUbi::TaGSK3* seedling leaves using extraction buffer containing 50 mM Tris-HCl (pH 8.0), 50 mM MES, 0.5 M sucrose, 1 mM $MgCl_2$, 20 mM EDTA, 5 mM DTT, and 1 mM PMSF. Purified Rht-A1, TaPROG1, or TaLA1-D fusion proteins (5 μg) were incubated with 1 mL of total protein extract supplemented with 10 mM ATP (Takara, 4041) at 25°C. Aliquots were collected at specified time intervals, heat-denatured (95°C, 5 min), and subjected to immunoblot analysis. Target proteins were detected using anti-His (1:3,000; CWBIO, CW0285M) or anti-MBP (1:2,000; ABclonal, AE075) antibodies, with RPN6 (1:2,000; ABclonal, A20512) as the loading control.

In vitro phosphorylation assay

Kinase reactions were performed in 20 μL volumes containing 1 μg GSK3-GST and 2 μg TaLA1^{C} or TaLA1^{N} fusion proteins in reaction buffer (25 mM Tris-HCl pH 7.5, 12 mM $MgCl_2$, 1 mM DTT, 1 mM ATP) at 37°C for 1 h, with GST alone as negative control. Reactions were terminated by adding 5 × SDS sample buffer. Phosphorylated proteins were resolved on 8% SDS-PAGE gels containing 50 μM Phos-tag (NARD, AAL-107) and

100 μM $MnCl_2$. Gels were sequentially washed with transfer buffer containing 1 mM EDTA (3 × 10 min) and EDTA-free buffer (1 × 10 min) before electroblotting onto PVDF membranes. Phosphorylation signals were detected using anti-MBP antibody (1:2,000; ABclonal, AE075).

Haplotype and selective signal analysis of *TaLA1-D*

The *TaLA1-D* gene, including 3 kb promoter region, exons and introns, were amplified and sequenced from all the 83 diverse wheat accessions. According to the sequence variants in the promoter region, the Hap1, Hap2 and Hap3 haplotypes were identified. Then we extended this analysis to 1351 wheat accessions from the wheat resequencing project[3,28-31]. Nucleotide diversity (π) and population differentiation (F_{ST}) were calculated in sliding windows across the genome using vcftools (π: 5-kb windows with a 1-kb step; F_{ST}: 20-kb windows with a 10-kb step). The wheat accessions are listed in Supplementary Data 6. The primers used for PCR are listed in Supplementary Data 7.

Statistics and reproducibility

Each experiment was repeated independently at least three times and similar experimental results were obtained. The results from one replicate are shown in the figures. Data are presented in the form of mean ± SD. Means of two samples were compared using Student's two-tailed *t* test. Multiple comparisons were compared by one way ANOVA with Duncan's multiple range tests. GraphPad Prism 10.2.3, SPSS 25 (Statistical Package for the Social Sciences) and Microsoft Excel 2016 were used for the statistical analyses.

Reporting summary

Further information on research design is available in the Nature Portfolio Reporting Summary linked to this article.

Data availability

The RNA sequencing data generated in this study have been deposited in the NCBI Sequence Read Archive (SRA) under BioProject accession code PRJNA1404857. All other data generated in this study are provided in the Supplementary Information and Source Data file. Source data are provided with this paper.

References

1. Appels, R. et al. Shifting the limits in wheat research and breeding using a fully annotated reference genome. *Science* **361** (2018).
2. Xiao, J. et al. Wheat genomic study for genetic improvement of traits in China. *Sci. China Life Sci.* **65**, 1718-1775 (2022).
3. Cheng, S. et al. Harnessing landrace diversity empowers wheat breeding. *Nature* **632**, 823-831 (2024).
4. Yao, Y. *et al.* Wheat2035: Integrating pan-omics and advanced biotechnology for future wheat design. *Mol. Plant* **18**, 272-297 (2025).
5. Peng, J. et al. 'Green revolution' genes encode mutant gibberellin response modulators. *Nature* **400**, 256-261 (1999).
6. Wang, Y. & Li, J. Rice, rising. *Nat. Genet.* **40**, 1273-1275 (2008).
7. Gao, H., Wang, W., Wang, Y. & Liang, Y. Molecular mechanisms underlying plant architecture and its environmental plasticity in rice. *Mol. Breeding* **39**, 167 (2019).
8. Wang, W., Gao, H., Liang, Y., Li, J. & Wang, Y. Molecular basis underlying rice tiller angle: current progress and future perspectives. *Mol. Plant* **15**, 125-137 (2022).
9. Li, Z. et al. OsBRXL4 regulates shoot gravitropism and rice tiller angle through affecting LAZY1 nuclear localization. *Mol. Plant* **12**, 1143-1156 (2019).
10. Xu, R. & Sun, C. What happened during domestication of wild to cultivated rice. *Crop J.* **9**, 564-576 (2021).
11. Waite, J.M. & Dardick, C. The roles of the IGT gene family in plant architecture: past, present, and future. *Curr. Opin. Plant Biol.* **59**, 101983 (2021).
12. Basu, U. & Parida, S.K. Restructuring plant types for developing tailor-made crops. *Plant Biotechnol. J.* **21**, 1106-1122 (2023).
13. Li, P. et al. *LAZY1* controls rice shoot gravitropism through regulating polar auxin transport. *Cell Res.* **17**, 402-410 (2007).
14. Yu, B. et al. *TAC1*, a major quantitative trait locus controlling tiller angle in rice. *Plant J.* **52**, 891-898 (2007).
15. Yin, T. et al. Precise tiller angle control by manipulating *TAC1* expression in rice. *J. Integr. Plant*

Biol. **67**, 1444-1446 (2025).
16. Jin, J. et al. Genetic control of rice plant architecture under domestication. *Nat. Genet.* **40**, 1365-1369 (2008).
17. Tan, L. et al. Control of a key transition from prostrate to erect growth in rice domestication. *Nat. Genet.* **40**, 1360-1364 (2008).
18. Wang, H. *et al*. Photoperiod and gravistimulation-associated *Tiller Angle Control 1* modulates dynamic changes in rice plant architecture. *Theor. Appl. Genet*. **136**, 160 (2023).
19. Wang, J. *et al.* Rice domestication-associated transcription factor PROSTRATE GROWTH 1 controls plant and panicle architecture by regulating the expression of *LAZY 1* and *OsGIGANTEA*, respectively. *Mol. Plant* **16**, 1413-1426 (2023).
20. Chen, X. et al. Genetic basis of tillering angle from other plants to wheat: current progress and future perspectives. *Plants* **13**, 3237 (2024).
21. Shaheen, A. et al. Genetic regulation of wheat plant architecture and future prospects for its improvement. *New Crops* **2**, 100048 (2025).
22. Zhao, D. et al. Identification and validation of genetic loci for tiller angle in bread wheat. *Theor. Appl. Genet.* **133**, 3037-3047 (2020).
23. Zhao, L. et al. A *HST1-like* gene controls tiller angle through regulating endogenous auxin in common wheat. *Plant Biotechnol. J.* **21**, 122-135 (2023).
24. Chen, Y. et al. Two open reading frames of *Rht-B1b* acting as brake and throttle contributed to wheat Green Revolution. *Plant Physiol.* **194**, 1290-1293 (2024).
25. Dong, H. et al. GSK3 phosphorylates and regulates the Green Revolution protein Rht-B1b to reduce plant height in wheat. *Plant Cell* **35**, 1970-1983 (2023).
26. Cao, J. et al. Natural variation of STKc_GSK3 kinase TaSG-D1 contributes to heat stress tolerance in Indian dwarf wheat. *Nat. Commun.* **15**, 2097 (2024).
27. Xiang, Y. et al. The maize GSK3-like kinase ZmSK1 negatively regulates drought tolerance by phosphorylating the transcription factor ZmCPP2. *Plant Cell* **37**, (2025).
28. Hao, C. et al. Resequencing of 145 landmark cultivars reveals asymmetric sub-genome selection and strong founder genotype effects on wheat breeding in China. *Mol. Plant* **13**, 1733-1751 (2020).
29. Guo, W. et al. Origin and adaptation to high altitude of Tibetan semi-wild wheat. *Nat. Commun.* **11**, 5085 (2020).
30. Zhou, Y. et al. *Triticum* population sequencing provides insights into wheat adaptation. *Nat. Genet.* **52**, 1412-1422 (2020).
31. Niu, J. et al. Whole-genome sequencing of diverse wheat accessions uncovers genetic changes during modern breeding in China and the United States. *Plant Cell* **35**, 4199-4216 (2023).
32. Zhang, H. *et al*. PROG1 acts upstream of LAZY1 to regulate rice tiller angle as a repressor. *Crop J.* **11**, 386-393 (2023).
33. Sasaki, A. *et al*. Green revolution: a mutant gibberellin-synthesis gene in rice. *Nature*. **416**:701-702 (2002).
34. Hu, S. *et al*. Xiaowei, a new rice germplasm for large-scale indoor research. *Mol. Plant* **11**:1418-1420 (2018).
35. Liao, Z. *et al*. SLR1 inhibits MOC1 degradation to coordinate tiller number and plant height in rice.

Nat. Commun. **10**:2738 (2019).
36. Dong, H. et al. A novel tiller angle gene, *TAC3*, together with *TAC1* and *D2* largely determine the natural variation of tiller angle in rice cultivars. *PLoS Genet.* **12**, e1006412 (2016).
37. Ausubel, F.M. et al. OsLIC, a novel CCCH-type zinc finger protein with transcription activation, mediates rice architecture via brassinosteroids signaling. *PLoS ONE* **3** (2008).
38. Cram, D. et al. WheatCRISPR: a web-based guide RNA design tool for CRISPR/Cas9-mediated genome editing in wheat. *BMC Plant Biol.* **19**, 474 (2019).
39. Dong, C. et al. *Tiller Number1* encodes an ankyrin repeat protein that controls tillering in bread wheat. *Nat. Commun.* **14**, 836 (2023).
40. Yoo, S.D., Cho, Y.H. & Sheen, J. *Arabidopsis* mesophyll protoplasts: a versatile cell system for transient gene expression analysis. *Nat. Protoc.* **2**, 1565-1572 (2007).

Acknowledgements

We would like to thank Aimin Zhang (Hebei Agricultural University) for kindly providing the gene-edited mutant of *TaGA3ox2*, Qixin Sun and Zhongfu Ni (China Agricultural University) for kindly providing the CRISPR/Cas9 system. We are grateful to Lingli Zheng and Wuman Xu for their excellent technical support.

Funding Statement

This work was supported by the Innovation Program of the Chinese Academy of Agricultural Sciences (CAAS-CSCB-202401 to L.Z., CAAS-ZDRW202403 to L.Z., CAAS-CSAL-202401 to J.S.), the National Natural Science Foundation of China Grant (31991213 to X.K., 32501899 to Y.C.), the Basic Research Center of Chinese Academy of Agricultural Sciences (CAAS-BRC-CS-2025-01, CAAS-BRC-202609) and the National Key Research and Development Program of China (2023YFD1200403).

Author contributions

X.K., J.S., L.Z. and X.L. conceived and designed the project; Y.C., Z.X., C.D., D.L., H.C. and B.L. performed the experiments and analyzed the data; C.X. provided suggestions on experiments; Y.C., J.S., X.K., L.Z., and X.L. wrote and revised the manuscript. All authors accepted the final version of the manuscript.

Competing interests

The authors declare no competing interests.

Figure legends

Fig. 1 | EMS-mutagenized mutants *ta1* and *ta2* exhibit increased tiller angles. a Phenotypic comparison between *ta1* mutant and wild-type YZ4110 plants. **b** Phenotypic comparison between *ta2* mutant and wild-type HM33 plants. **c, d** Quantitative analysis of tiller angle (**c**) and plant height (**d**) in *ta1* and YZ4110 (mean ± SD, *n* = 10 biological samples). **e, f** Shoot gravity response and statistical analysis of *ta1* and YZ4110 seedlings after gravity stimulation for 48 h. Data represent mean ± SD (*n* = 10 biological samples). Scale bar: 2 cm. **g, h** Quantitative analysis of tiller angle (**g**) and plant height (**h**) in *ta2* and HM33 (mean ± SD, *n* = 10 biological samples). **i, j** Shoot gravity response and statistical analysis of *ta2* and HM33 seedlings after 48 h gravistimulation. Data represent mean ± SD (*n* = 10 biological samples). Scale bar, 2 cm. $^{**}P < 0.01$ (two-tailed Student's *t*-test).

Fig. 2 | Map-based cloning showed that *TA1* encodes the DELLA protein Rht-A1. a Distribution of SNPs with biased allele frequencies across 21 wheat chromosomes, genotyped using the wheat 55K SNP array. **b–d** Fine-mapping of the *TA1* candidate gene. **e** *In vitro* degradation assays comparing Rht-A1 and Rht-A1^{ta1} proteins. Representative images from three independent experiments are shown. **f, g** Phenotypic characterization of *pRht-A1::Rht-A1^{ta1}* and *pUbi::Rht-A1^{ta1}-Flag* transgenic wheat plants (scale bar, 10 cm). **h** Genetic effects among *Rht-A1^{ta1}*, *Rht-B1b* and *Rht-D1b* alleles (scale bar, 10 cm). **i, j** Quantitative analysis of tiller angle (**i**) and plant height (**j**) in different *Rht-1* allelic combinations. Data represent mean ± SD (*n* = 12 biological samples). Different lowercase

letters denote statistically significant differences (P < 0.05, one-way ANOVA with Duncan's multiple range test).

Fig. 3 | Molecular cloning and functional characterization of *TaLA1-D*. a Distribution of frequency-biased SNPs across wheat chromosomes using the 55 K SNP array. **b** Map-based cloning of the *TA2* candidate gene. *TaLA1-D* (*TraesCS6D02G396500*) was identified as the candidate gene, containing a G to A mutation in the coding region. **c** Semi-*in vivo* degradation assays of TaLA1-D and TaLA1-D^{ta2} proteins detected by anti-His antibody, with RPN6 as loading control. Representative images from three independent experiments are shown. The intensity values of the protein levels were detected by Image J. **d** Tiller angle phenotypes of CRISPR-generated *Tala1* mutants (scale bar, 10 cm). **e** Quantitative analysis of tiller angles (mean ± SD, n = 10 biological samples). **f** Quantification of auxin levels in the tiller base of *CRISPR-Tala1* mutants compared to the wild-type (WT) control. **g, h** RT–qPCR analysis of *TaEXPB7* (**g**) and *TaXTH19* (**h**) expression in the tiller base of *CRISPR-Tala1* mutants and WT plants. In **f-g** data are mean ± SD; n = 3 biological replicates. **P < 0.01 (two-tailed Student's t-test).

Fig. 4 | Rht-A1 interacts with TaPROG1 to synergistically repress the expression of *TaLA1-D* in the regulation of wheat tiller angle. a *TaLA1-D* expression in YZ4110 versus *ta1* mutants (mean ± SD, n = 3 biologically independent replicates). **b** Schematic of dual-luciferase reporter and effector vector. **c** Transcriptional repression of *TaLA1-D* promoter by TaPROG1 in protoplasts (mean ± SD, n = 3 biologically independent replicates). **d, e** Protein-protein interaction between Rht-A1 and TaPROG1 demonstrated by LCI (**d**) and BiFC (**e**) assays (scale bars, 50 μm; YFP, yellow fluorescent protein). Representative images from three independent experiments are shown. **f** Tiller angle phenotype of *Rht-A1^{ta1}*/*TaPROG1* plants (scale bar, 10 cm). **g** Cooperative repression of

TaLA1-D by Rht-A1 and TaPROG1 (mean ± SD, *n* = 3 biologically independent replicates). Two-tailed Student's *t*-test; ***P* < 0.01 for all statistical analyses.

Fig. 5 | TaGSK3-mediated phosphorylation stabilizes TaLA1-D to regulate wheat tiller angle. a Phenotypic characterization of *pUbi::TaGSK3* transgenic wheat plants showing compact architecture. Scale bar: 10 cm. **b** Comparative analysis of tiller angle between wild-type KN199 and *pUbi::TaGSK3* overexpression lines. Data represent mean ± SD (*n* = 10 biological samples). **c–e** Protein-protein interaction validation between TaLA1-D and TaGSK3 through yeast two-hybrid (Y2H) (**c**), luciferase complementation imaging (LCI) assays (**d**) and bimolecular fluorescence complementation (BiFC) (**e**) (YFP signal shown; scale bars, 50 μm). Representative images from three independent experiments are shown. **f** *In vitro* phosphorylation assay demonstrating TaGSK3-dependent phosphorylation of TaLA1-D fragments (TaLA1-D^{N}: residues 1-250; TaLA1-D^{C}: residues 101-384). Phosphorylated bands (*) were detected using anti-MBP antibody. Representative images from three independent experiments are shown. **g** Cell-free degradation assays comparing protein stability of TaLA1-D versus phosphorylation-deficient mutant TaLA1-D^{ta2}. Anti-His and anti-RPN6 (loading control) antibodies were used for detection. Representative images from three independent experiments are shown. **h**, **i** Tiller angle phenotypes of three lines: the *TaGSK3*^{E286K}-overexpression line (OE), the same overexpression in the *CRISPR-Tala1* background, and the *CRISPR-Tala1* mutant. The tiller angles of the latter two lines did not differ significantly from each other but were both significantly greater than that of the OE line alone. Scale bar, 10 cm. Data are mean ± SD (*n* = 10 biological samples). ***P* < 0.01 (two-tailed Student's *t*-test for indicated comparisons).

Fig. 6 | *TaLA1-D*^{Hap1} has been significantly selected during wheat breeding. a Genetic classification of three *TaLA1-D* haplotypes (Hap1–Hap3) based on 5 SNPs. **b**

Haplotype frequency variations between 50 wheat landraces and 33 modern cultivars, showing significant enrichment of Hap1 in improved varieties. **c–f** Agronomic trait comparisons across haplotypes: tiller angle (**c**), grain width (**d**), grain length (**e**) and thousand kernel weight (**f**). Data are mean ± SD. Letters indicate statistical significance ($P < 0.05$, one-way ANOVA with Duncan's test).

Fig. 7 | A working model for the *Rht-A1–TaLA1-D* module in controlling wheat tiller angle. The Rht-A1/TaPROG1 complex transcriptionally represses *TaLA1-D* expression, whereas TaGSK3 stabilizes TaLA1-D protein via phosphorylation, forming a balanced regulatory module. This balance dictates tiller angle: enhanced repression (as in the *ta1* mutant) or loss of *TaLA1-D* leads to enlarged tiller angles; conversely, enhanced TaLA1-D stabilization (the $Tagsk3^{E286K}$ mutant/transgenic plants) promotes a compact architecture with reduced tiller angles.

Editorial Summary:

This study identifies a Rht-A1–TaLA1-D module controlling wheat tiller angle, elucidates its mechanism, and traces the selection trajectory of TaLA1-D during wheat breeding, providing new insights for developing ideotype wheat varieties.

Peer Review Information*: Nature Communications* thanks Hailiang Mao, Lubin Tan and Shengbao Xu who co-reviewed with Chao Zhang for their contribution to the peer review of this work. A peer review file is available.

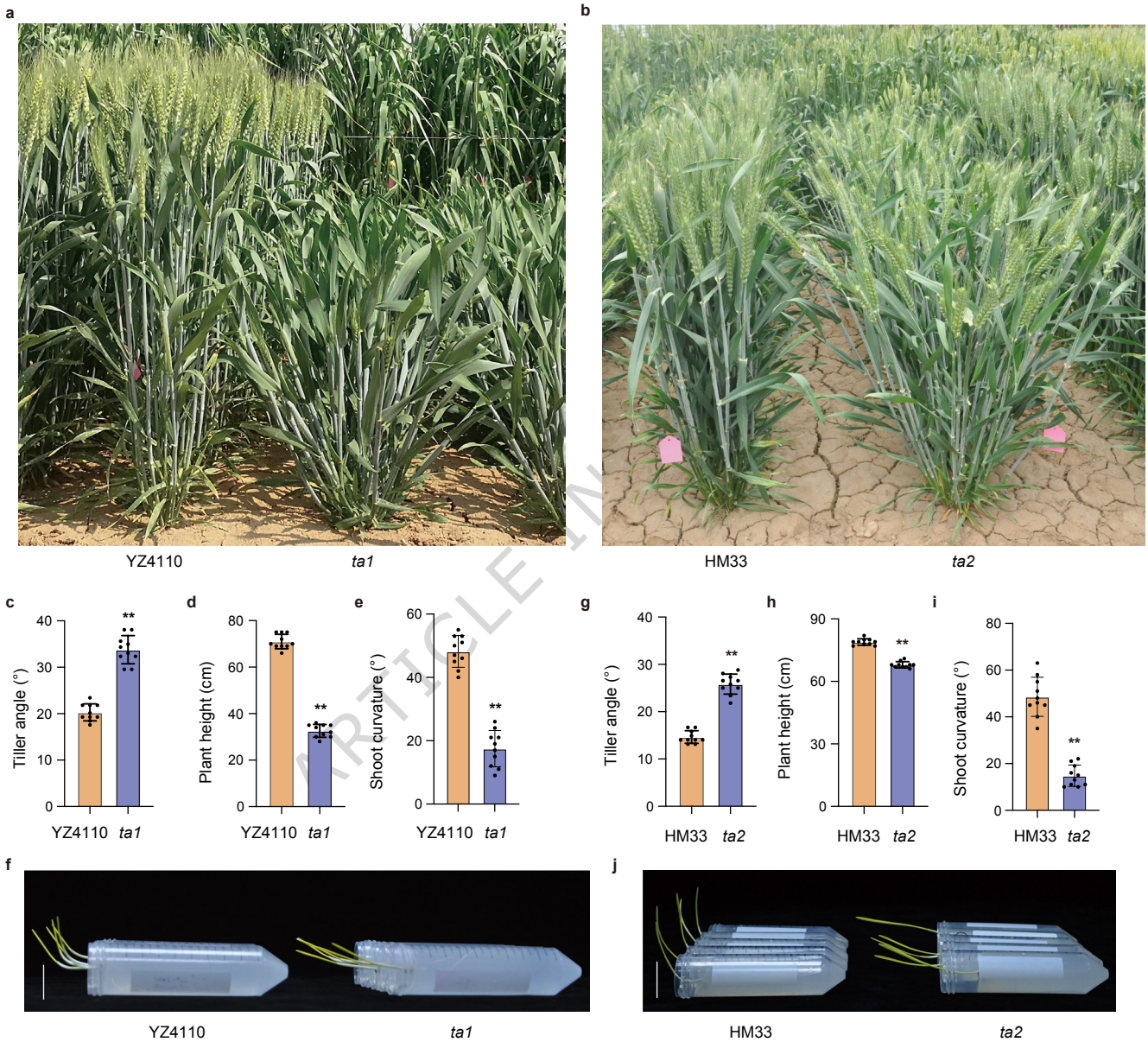

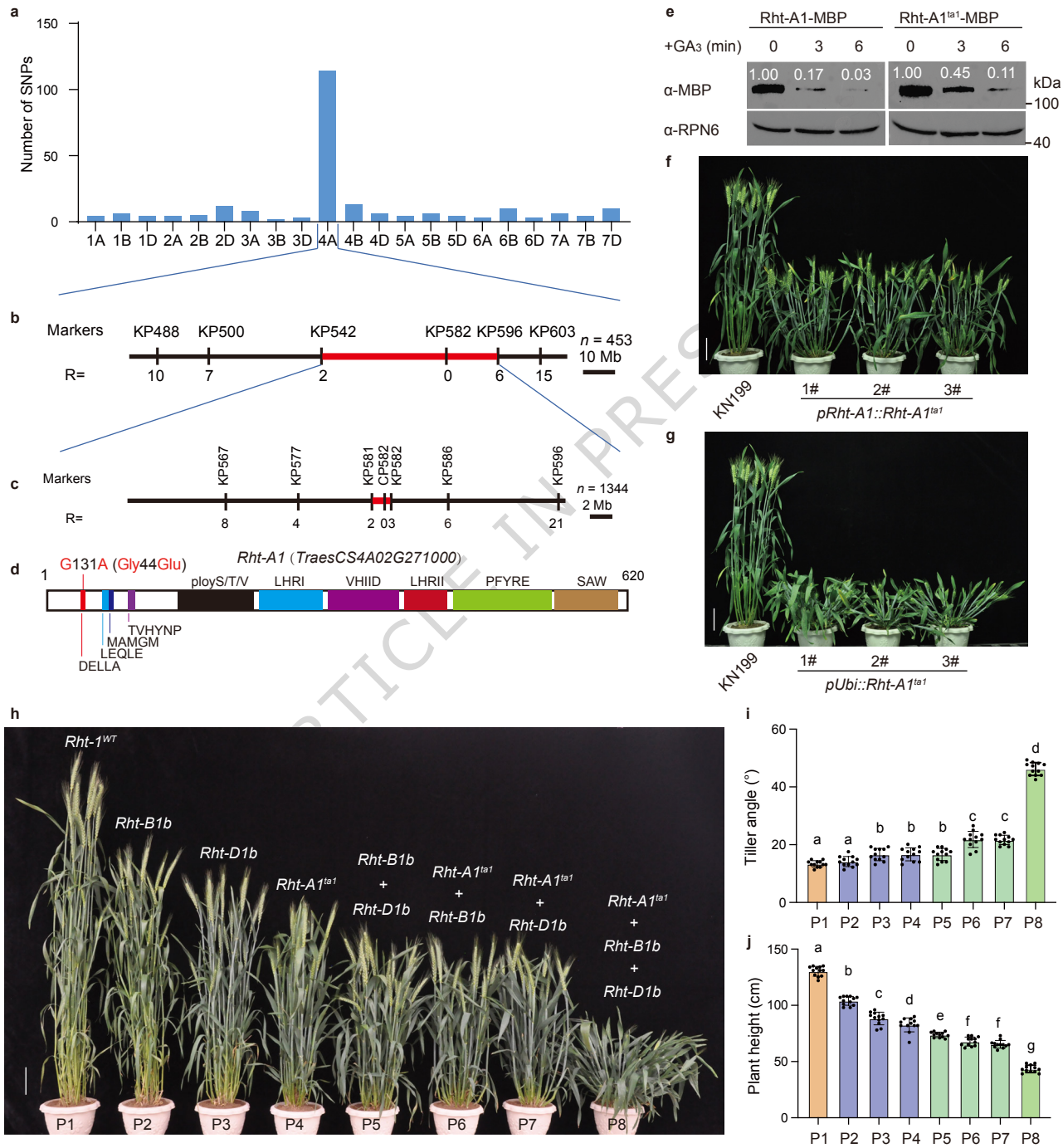
a
Number of SNPs
150
100
50
0
1A 1B 1D 2A 2B 2D 3A 3B 3D 4A 4B 4D 5A 5B 5D 6A 6B 6D 7A 7B 7D
b
Markers
KP488 KP500 KP542 KP582 KP596 KP603
n = 453
10 Mb
R=
10 7 2 0 6 15
c
Markers
KP567 KP577 KP581 CP582 KP582 KP586 KP596
n = 1344
2 Mb
R=
8 4 2 03 6 21
d
1
G131A (Gly44Glu)
Rht-A1 (TraesCS4A02G271000)
ployS/T/V LHRI VHIID LHRII PFYRE SAW
620
TVHYNP
MAMGM
LEQLE
DELLA
e
Rht-A1-MBP
Rht-A1ta1-MBP
+GA3 (min) 0 3 6 0 3 6
1.00 0.17 0.03
1.00 0.45 0.11
α-MBP
α-RPN6
kDa
100
40
f
KN199
1# 2# 3#
pRht-A1::Rht-A1ta1
g
KN199
1# 2# 3#
pUbi::Rht-A1ta1
h
Rht-1WT
Rht-B1b
Rht-D1b
Rht-A1ta1
Rht-B1b + Rht-D1b
Rht-A1ta1 + Rht-B1b
Rht-A1ta1 + Rht-D1b
Rht-A1ta1 + Rht-B1b + Rht-D1b
P1 P2 P3 P4 P5 P6 P7 P8
i
Tiller angle (°)
60
40
20
0
a a b b b c c d
P1 P2 P3 P4 P5 P6 P7 P8
j
Plant height (cm)
150
100
50
0
a b c d e f f g
P1 P2 P3 P4 P5 P6 P7 P8

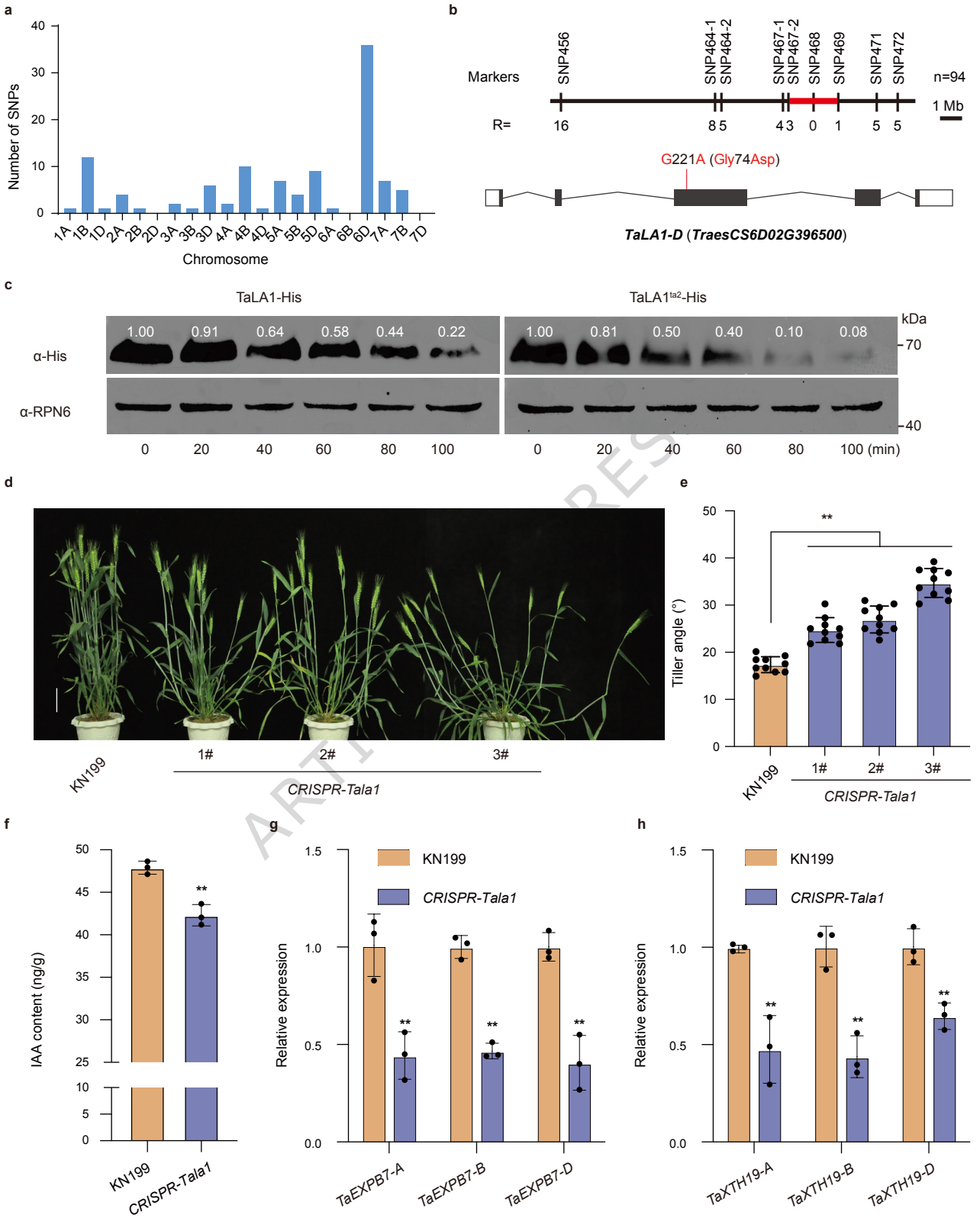
a
Number of SNPs
Chromosome
1A 1B 1D 2A 2B 2D 3A 3B 3D 4A 4B 4D 5A 5B 5D 6A 6B 6D 7A 7B 7D
b
Markers
SNP456
SNP464-1
SNP464-2
SNP467-1
SNP467-2
SNP468
SNP469
SNP471
SNP472
n=94
1 Mb
R=
16
8 5
4 3
0
1
5
5
G221A (Gly74Asp)
TaLA1-D (TraesCS6D02G396500)
c
TaLA1-His
TaLA1ta2-His
kDa
α-His
α-RPN6
1.00 0.91 0.64 0.58 0.44 0.22
1.00 0.81 0.50 0.40 0.10 0.08
70
40
0 20 40 60 80 100
0 20 40 60 80 100 (min)
d
KN199
1#
2#
3#
CRISPR-Tala1
e
Tiller angle (°)
**
KN199
1#
2#
3#
CRISPR-Tala1
f
IAA content (ng/g)
**
KN199
CRISPR-Tala1
g
Relative expression
KN199
CRISPR-Tala1
**
TaEXPB7-A
TaEXPB7-B
TaEXPB7-D
h
Relative expression
KN199
CRISPR-Tala1
**
TaXTH19-A
TaXTH19-B
TaXTH19-D

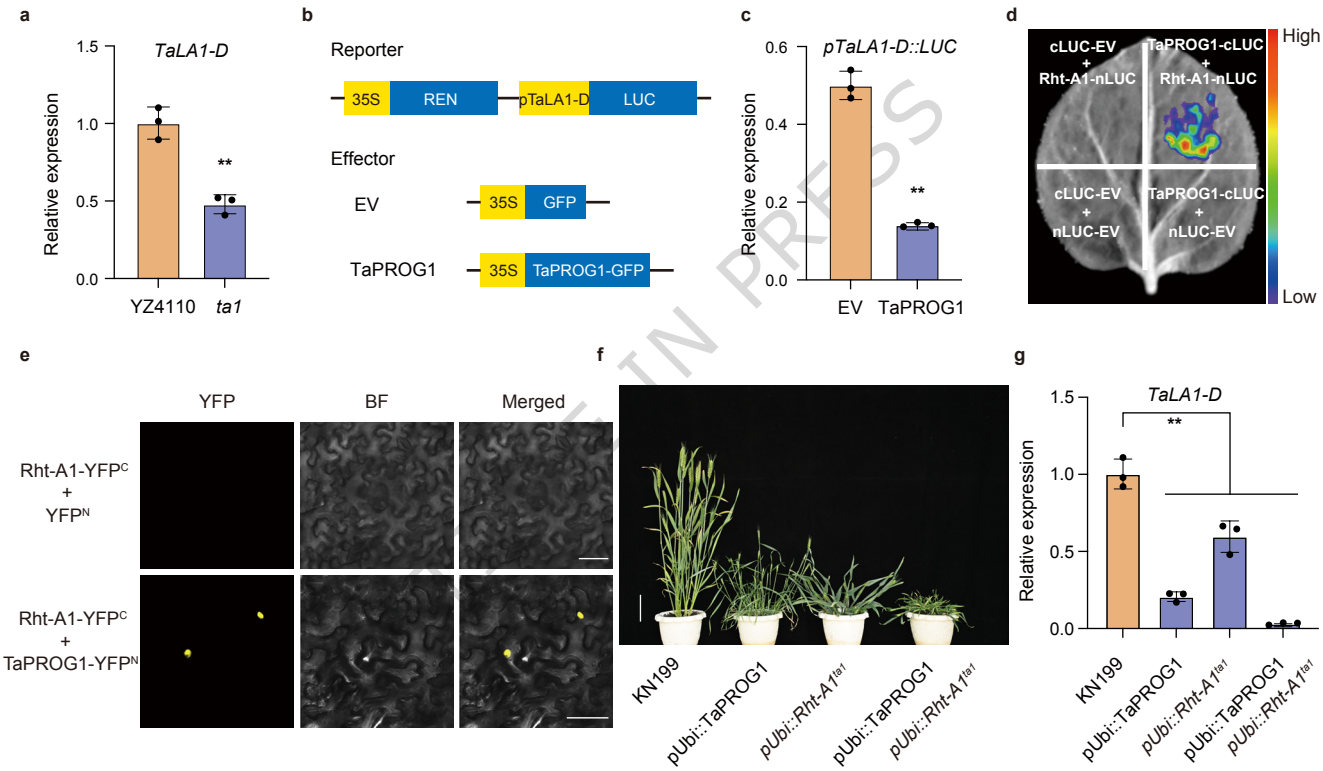

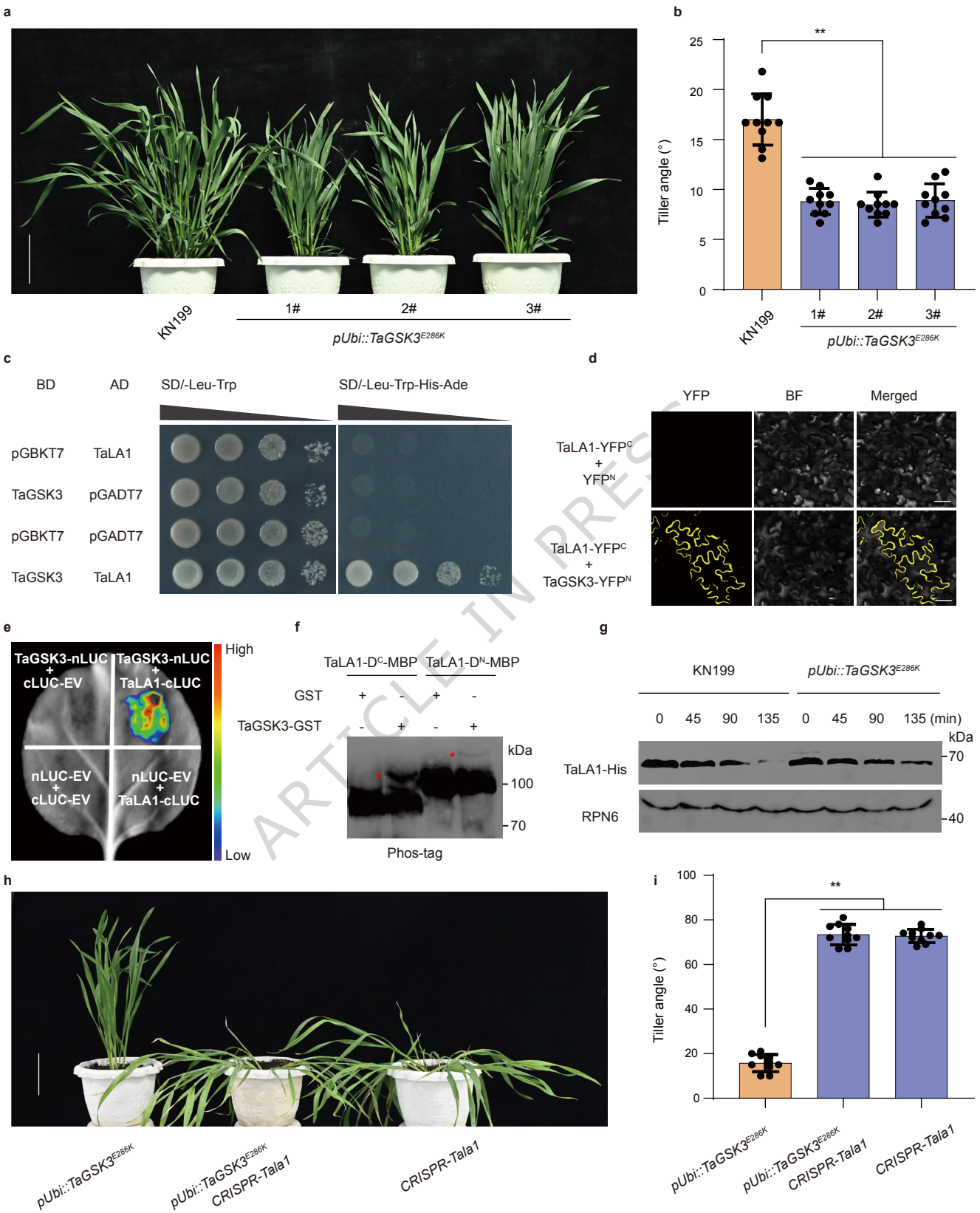

a

Haplotype	-2583	-2549	-2463	-2156	-1675
Hap1	G	C	C	A	T
Hap2	G	C	C	A	A
Hap3	T	G	T	G	A

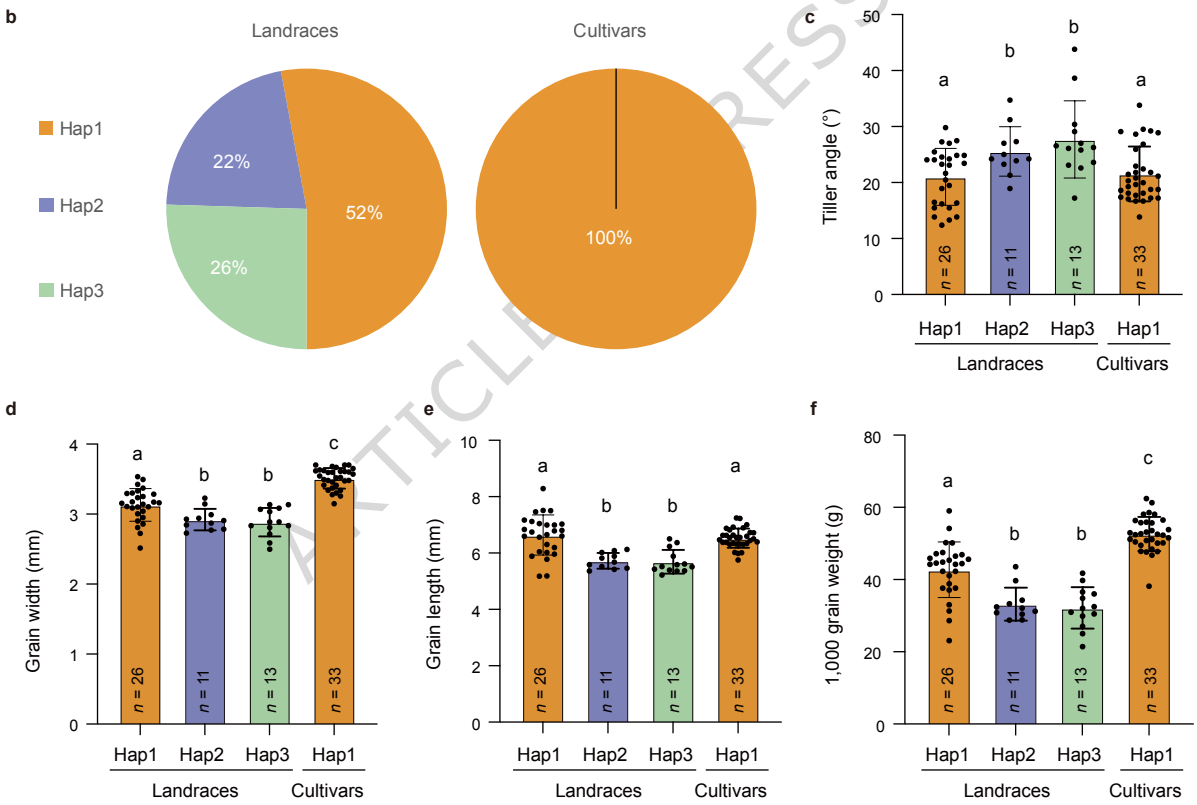

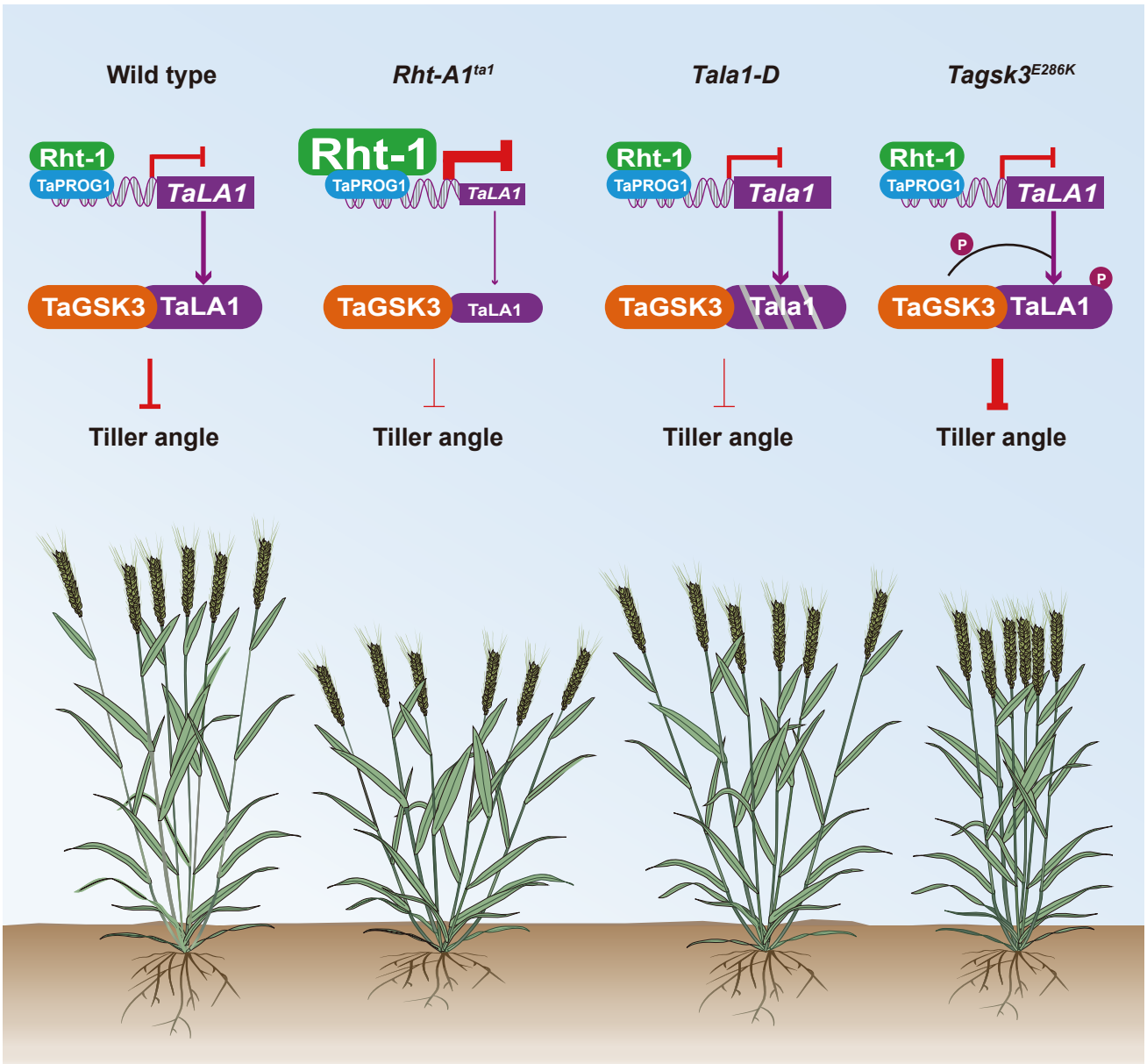
Wild type
Rht-A1ta1
Tala1-D
Tagsk3E286K
Rht-1
TaPROG1
TaLA1
TaGSK3
TaLA1
Rht-1
TaPROG1
TaLA1
TaGSK3
TaLA1
Rht-1
TaPROG1
Tala1
TaGSK3
Tala1
Rht-1
TaPROG1
TaLA1
P
TaGSK3
TaLA1
P
Tiller angle
Tiller angle
Tiller angle
Tiller angle